Effect of palladium doping on structural and optical properties of WO_3 nanostructures

Jasmeet Kaur[1,*], Kanica Anand[1], Anita Hastir[1], Virpal[1], Amanpreet Kaur[1] and Ravi Chand Singh[1,*]

Abstract— In this work, the effect of palladium (Pd) as dopant on the structural and optical properties of WO_3 nanostructures has been discussed. Pure and Pd (0.5 %, 1 % and 1.5 %) doped WO_3 nanostructures were synthesized by acid precipitation method. XRD analysis with Rietveld refinement revealed the formation of monoclinic phase for WO_3 and Pd doped WO_3 nanostructures which were further supported by Raman studies. It was observed that the crystallite size of WO_3 nanostructures was decreased with increase in Pd concentration. FESEM micrographs showed nanoplate type morphology of pure and Pd doped WO_3 nanostructures. EDX confirmed the presence of Pd dopant in WO_3 nanostructures. A broadening and shifting of Raman stretching modes in Pd doped WO_3 nanostructures was observed. Diffuse reflectance spectroscopy results showed a red shift in band gap with Pd doping. Photoluminescence spectra exhibited blue and violet emission which was due to direct band transition and oxygen vacancies. A small shift in the peaks of violet and blue emission with Pd doping was also observed and attributed to defect centres created with doping.

Index Terms— Doping, Nanoplates, Photoluminescence, Rietveld refinement, Raman spectroscopy, Sensor, WO_3.

1 Introduction

Tungsten trioxide (WO_3) is a fascinating material, which shows outstanding properties for applications in several important technologies, such as gas sensors, solar cells and photocatalysis [1], [2], [3], [4]. These applications strongly depend upon structural, optical and morphological features [5]. Doping is one of the most effective and proficient method to alter these properties [6]. For example, Bai *et al.* reported enhanced acetone sensitive properties of copper-doped WO_3 sensors in comparison to pristine WO_3 [7]. Feng *et al.* showed that Ti doped WO_3 nanostructures exhibited improved visible-light-driven photocatalytic properties [8].

Moreover, the decoration of noble metals such as palladium (Pd) and platinum (Pt) offers a high surface area, fast gas diffusion and mass transport kinetics to WO_3 based gas sensors due to their fascinating catalytic properties [9], [10]. Recently, Wang *et al.* demonstrated that existence of Pd on the WO_3 surface boosts the sensitivity of the sensor and lowers the optimum operating temperature at low concentrations of hydrogen gas [11]. However, the synthesis of the noble metal Pd doped WO_3 nanoplates have rarely explored.

In this paper, we report the effect of Pd as doping on the structural and optical properties of WO_3 nanostructures. The study of structural and optical properties of Pd doped WO_3 have immense importance for device applications.

2 Experimental

2.1 Synthesis

In the synthesis of WO_3 nanostructures, $Na_2WO_4 \cdot 2H_2O$ was dissolved into distilled water and nitric acid taken both in equal volume to prepare 0.2 M solution. The solution was kept on stirring continuously for 4 h at room temperature and then aged for 24 h. The obtained yellow precipitates of $WO_3.H_2O$ were filtered and washed thoroughly with distilled water and ethanol several times to remove any impurity ions. The expected chemical reaction was

$$Na_2WO_4 + HNO_3 \rightarrow H_2WO_4 + 2\,NaNO_3 \quad (1)$$

$$H_2WO_4 \rightarrow WO_3 + H_2O \quad (2)$$

The resulting precipitates were dried at 60°C in the oven which was followed by calcination at 500°C for 3h. Similarly, 0.5, 1.0 and 1.5 % Pd doped WO_3 nanostructures(labelled as 0.5Pd, 1Pd and 1.5 Pd, respectively) were prepared by adding appropriate amount of $PdCl_2$ to $Na_2WO_4 \cdot 2H_2O$ solution and following the above mentioned procedure.

2.2 Characterization

The crystal structure of the synthesized samples was studied by powder X-ray diffraction (XRD) (D8 Focus, BRUKER, Ettlingen, Germany) operated at 40 kV and 30 mA using Cu-$K_{\alpha 1}$ radiation. The morphology of samples were analysed by field emission scanning electron microscope (FESEM; Carl Zeiss SUPRA 55). Raman spectra were recorded at room temperature on a Renishaw Invia microscope with an argon-ion laser at an excitation wavelength of 514 nm. UV-Vis diffuse reflectance spectra (DRS) of samples were measured on a UV-Vis-NIR spectrophotometer (Shimadzu UV-3600 spectrophotometer). Photoluminescence spectra (PL) were recorded (Lambda 45, Perkin Elmer fluorescence spectrometer) at excitation wavelength of 310 nm.

3 Results and Discussion

3.1 XRD analysis

The XRD patterns of the WO_3 and Pd doped WO_3 nanostructures are shown in Fig. 1. The three prominent peaks corresponding to reflection planes (200), (020) and (002) of WO_3 are

- [1]*Department of Physics, Guru Nanak Dev University, Amritsar, India-143005, India*
- **Email: ravichand.singh@gmail.com, jasmeet.dayal@gmail.com*

present in XRD pattern which suggests the monoclinic phase [12] of as obtained WO_3 (JCPDS-83-0951). No trace of impurity peak associated with Pd is observed which may be due to low doping content of Pd. The absence of dopant peaks also confirms the successful incorporation of Pd into the WO_3 lattice. With Pd doping, the corresponding diffraction intensity also decreases which may be due to the lattice distortion induced by Pd ion into WO_3 crystal as the ionic radius of dopant ion is larger (ionic radii of Pd^{2+} and W^{6+} is 78 and 67 pm respectively) than host [13]. The crystallite size (D) has been calculated by employing the Scherrer's equation [14] and the values are listed in Table 1. A decrease in crystallite size has been observed on doping which reveals that incorporation of Pd into WO_3 might restrain the nanostructures growth to some extent.

Additionally, the Rietveld refinements of all samples have been performed on XRD data by employing Full Prof program. The refinements have been carried out with P 21/n space group for XRD patterns in a 2θ range of 10–70◦ with a step size 0.02◦. Fig. 2 represents Rietveld refined XRD patterns for WO_3 and Pd doped WO_3 nanostructures. The lattice parameters 'a', 'b', 'c'and 'β' and Chi-square values obtained from Rietveld analysis are presented in Table 1. Initially, the cell volume decreases (0.5 Pd), then it increases (1Pd) and finally it increases again (1.5 Pd). This deviation in cell volume of the Pd doped WO_3 nanostructures comparative to pure WO_3 are attributed to the presence of Pd ions into the WO_3 lattice network. Upadhyay *et al.* have reported similar variations in lattice parameters and cell volume for indium doped WO_3 [12].

3.2 Raman spectroscopy

To further investigate the chemical structure of WO_3 and Pd doped WO_3 nanostructures, the Raman spectra were recorded at room temperature. Fig. 3 displays the Raman spectra of WO_3 and Pd doped WO_3 nanostructures. Raman spectra of pure WO_3 nanostructure exhibit characteristics peaks at 808 and 715 cm^{-1} which are linked to the W-O-W stretching mode. The Raman bands correspond to O-W-O bending vibration modes are also observed at 327 and 275 cm^{-1} [12].

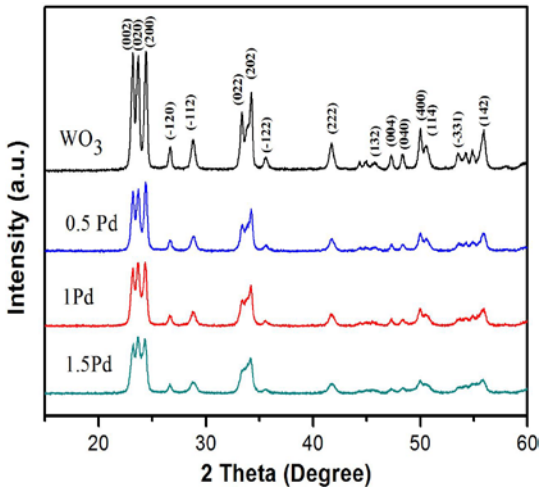

Fig. 1. XRD patterns of pure WO_3 and Pd doped WO_3 nanostructures.

With Pd doping, these bands become broad and shifts towards lower wavenumbers confirming the incorporation of dopant into WO_3 lattice. A relative decrease in intensity in Pd doped WO_3 nanostructures is also observed which is attributed to presence of structural disorder upon doping.

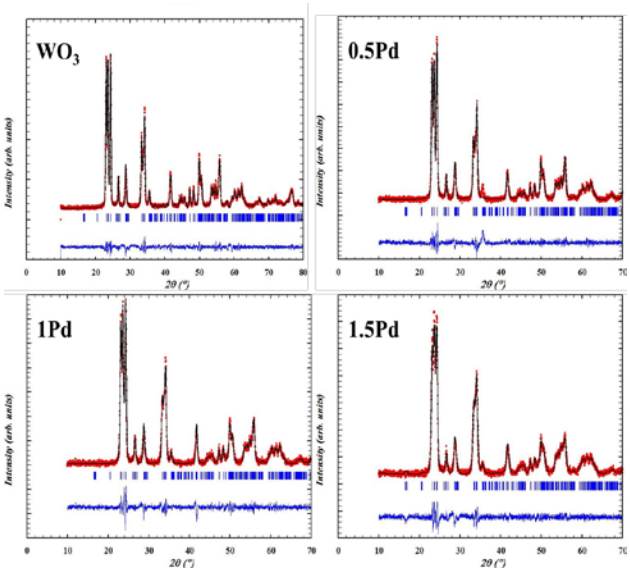

Fig. 2. Rietveld refinement plots of pure WO_3 and Pd doped WO_3 nanostructures.

3.3 FESEM-EDX analysis

After confirmation of monoclinic phase from XRD and Raman studies, FESEM measurements were employed to analyse the morphology of WO_3 and Pd doped WO_3 nanostructures. Fig.4 shows the FESEM micrographs of WO_3 and Pd doped WO_3 nanostructures which shows a compact distribution of nanosheets like morphology which are randomly aligned and overlapped. With doping, the thickness of sheets decreases which is in accordance with crystalline size variation as obtained from XRD data.

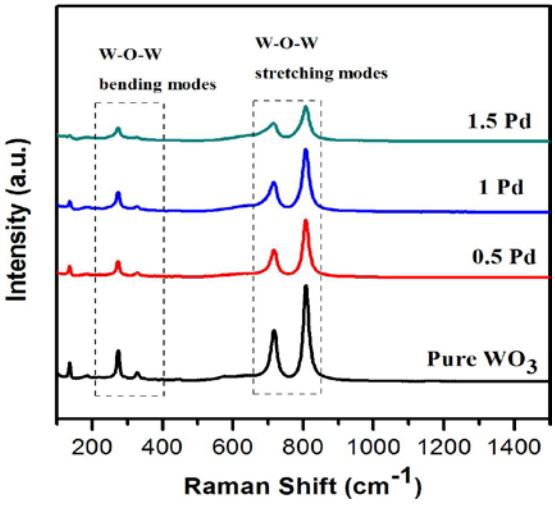

Fig. 3. Raman spectra of pure WO_3 and Pd doped WO_3 nanostructures.

The EDX analysis confirms the presence of Pd in WO_3 nanos-

tructures. Fig. 5 shows the EDX spectra of the WO_3 and 1Pd nanostructures. No other element except W, Pd and O has been detected which shows that final products are free of impurities.

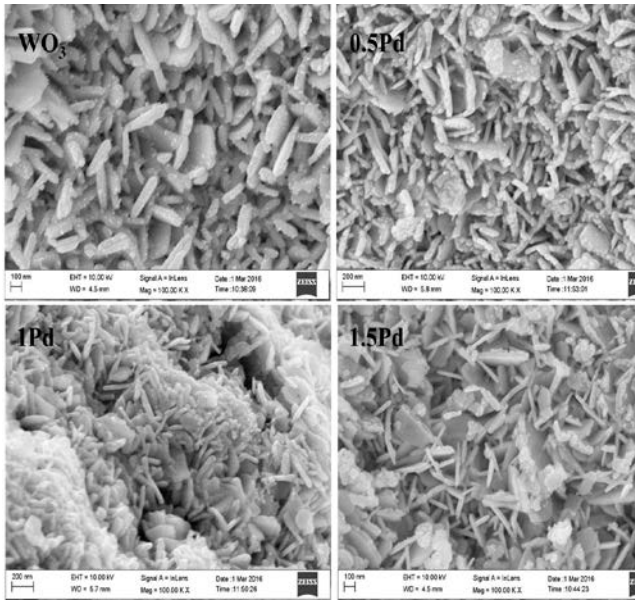

Fig. 4. FESEM micrographs of pure WO_3 and Pd doped WO_3 nanostructures showing nanoplate type morphology.

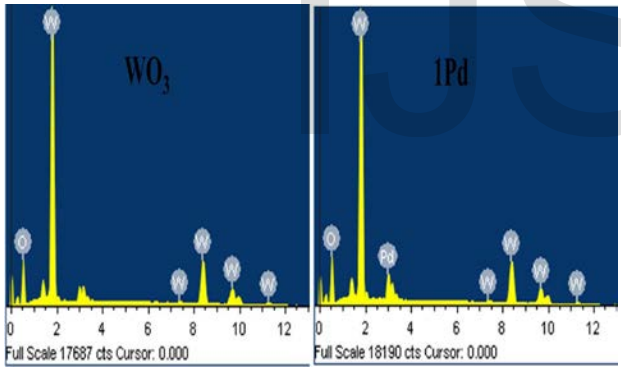

Fig. 5. EDX spectra of pure WO_3 and 1Pd doped WO_3 nanostructures.

3.4 DRS spectra

DRS spectra of WO_3 and Pd doped WO_3 nanostructures are shown in Fig. 6a. The absorption spectra of nanostructures are obtained by using Kulbeka Munk function [15]. A small blue shift in absorption spectra has been observed with Pd doping. By plotting $[F(R)^* h\nu]^2$ vs hν and extrapolating the linear part of the curve $[F(R)^* h\nu]^2$ to zero, the direct band gap energy (E_g) of WO_3 nanostructures has been determined (Fig. 6b) and the obtained E_g values are tabulated in Table 1. It can be seen that there is red shift in band gap with Pd doping. This optical band gap widening upon Pd doping can be attributed to presence of large numbers of oxygen vacancies which may lead to band filling effect. The difference in charge between dopant and host ions can be the reason behind band filling. Similar

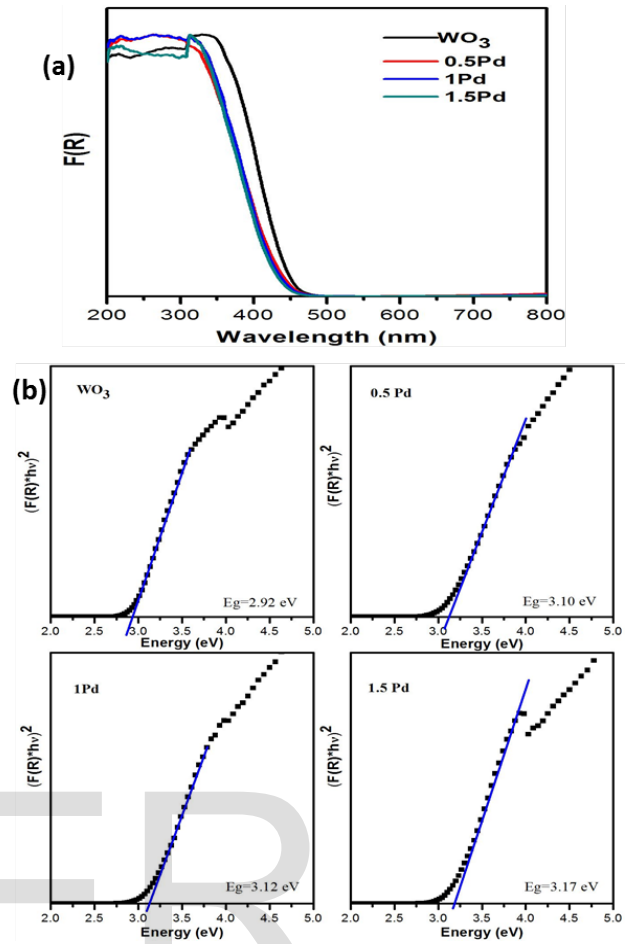

Fig. 6. (a) DRS absorption spectra and (b) $(F(R)^*h\nu)^2$ versus hν plots of pure WO_3 and Pd doped WO_3 nanostructures.

TABLE1

Crystallite size (D), Lattice parameters (a, b, c and β) extracted from Rietveld analysis and Band gap energy value (E_g) of pure WO_3 and Pd doped WO_3 nanostructures.

Sample	Crystallite size (nm)	Lattice parameters (Å)	Chi-square	Unit cell volume (Å)³	Band gap (eV)
WO₃	28.70	a=7.312 b=7.536 c=7.696 β=90.46	2.01	424.174	2.92
0.5Pd	18.89	a=7.316 b=7.528 c=7.689 β=90.44	1.79	423.522	3.10
1Pd	19.79	a=7.326 b=7.523 c=7.687 β=90.33	1.61	423.749	3.12
1.5Pd	18.04	a=7.333 b=7.516 c=7.681 β=90.63	1.55	423.380	3.17

decrease in band gap due to doping has been reported previously in literature [16].

3.4 PL spectra

Fig. 7 displays the PL spectra of WO_3 and Pd doped WO_3 nanostructures. The inset of Fig.7 displays the deconvoluted PL spectrum of WO_3 which shows deep level emission (DL) comprising of blue and violet emission which may be due to direct band transistion and oxygen vacancies. The intensity of DL emissions increases with increase of Pd in WO_3 which suggests the enhancement of defects with doping [16]. A small shift in the peaks of violet and blue emission with Pd doping has also been observed.

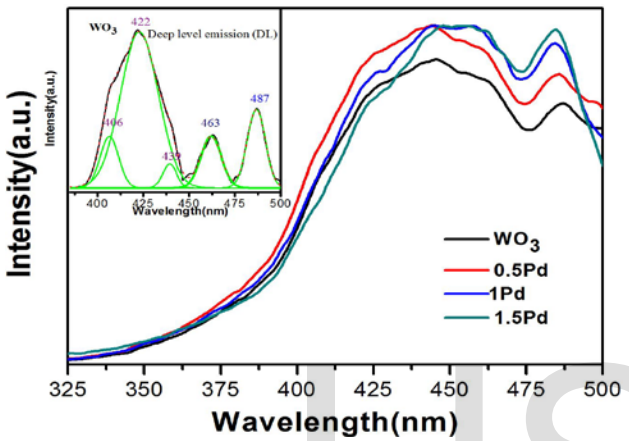

Fig. 7. PL spectra of pure WO_3 and Pd doped WO_3 nanostructures; inset showing deconvolution of pure WO_3.

4 CONCLUSION

In summary, we can write that doping of Pd into WO_3 lattice has been successfully achieved by simple cost effective acid precipitation method. XRD and Raman studies confirm the monoclinic phase of all samples. The decrease in crystallite size and variation in lattice constants with Pd doping is due to difference in ionic radii of dopant and host. The Raman modes in Pd doped WO_3 nanostructures becomes broad, comparative less intense and shifts towards lower frequencies in comparison to pure WO_3. FESEM micrographs reveal nanoplate type morphology of pure and Pd doped WO_3 nanostructures. A red shift in bandgap has been observed for Pd doped WO_3 nanostructures. The presence of oxygen vacancies/defects arises from Pd doping has been confirmed by enhanced PL emission intensity.

ACKNOWLEDGMENT

The authors gratefully acknowledge Central Instrumental Facility, Guru Nanak Dev University, Amritsar, India for providing all instrument facilities under UGC-UPE and DST-FIST schemes. Jasmeet Kaur wishes to thank UGC, India for providing fellowship in carrying out Ph.D research work.

REFERENCES

[1] A. Ponzoni, V. Russo, A. Bailini, C.S. Casari, M. Ferroni, A. L. Bassi, A. Migliori, V. Morandi, L. Ortolani, G. Sberveglieri and C.E. Bottani, "Structural And Gas-Sensing Characterization Of Tungsten Oxide Nanorods And Nanoparticles", *Sensors and Actuators B*, vol. 153, pp. 340–346, 2011.

[2] L. Meda, G. Tozzola, A. Tacca, G. Marra, S. Caramori, V. Cristino and C. A. Bignozzi, "Photo-Electrochemical Properties Of Nanostructured WO_3 Prepared With Different Organic Dispersing Agents", *Sol. Energy Mater. Sol. Cells*, vol. 94, pp. 788-796, 2010.

[3] D. Chen and J.H. Ye, "Hierarchical WO_3 Hollow Shells: Dendrite, Sphere, Dumbbell, And Their Photocatalytic Properties", *Adv. Funct. Mater.*, vol. 18, pp. 1922–1928, 2008.

[4] S. K. Deb, "Opportunities And Challenges In Science And Technology Of WO3 For Electrochromic And Related Applications", *Sol. Energy Mater. Sol. Cells*, vol. 92, pp. 245-258, 2008.

[5] D. Chen, X. Hou, T. Li, L. Yin, B. Fan, H. Wang, X. Li, H. Xu, H. Lu, R. Zhang and J. Sun, "Effects Of Morphologies On Acetone-Sensing Properties Of Tungsten Trioxide Nanocrystals", *Sensors and Actuators B*, vol. 153 pp. 373–381, 2011.

[6] W. Mu, X. Xie, X. Li, R. Zhang, Q. Yu, K. Lv, H. Wei and Y. Jian, "Characterizations Of Nb-Doped WO_3 nanomaterials And Their Enhanced Photocatalytic Performance", *RSC Adv.*, vol. 4, pp. 36064- 36070, 2014.

[7] X. Bai, H. Ji, P. Gao, Y. Zhang and X. Sun, "Morphology, Phase Structure And Acetone Sensitive Properties Of Copper-Doped Tungsten Oxide Sensors", *Sensors and Actuators B*, vol. 193, pp. 100-106, 2014.

[8] C. Feng, S. Wang and B. Geng, "Ti(IV) Doped WO_3 Nanocuboids: Fabrication And Enhanced Visible-Light-Driven Photocatalytic Performance", Nanoscale, vol. 3, pp. 3695- 3699, 2011.

[9] P. V. Tong, N. D. Hoa, N. V. Duy, D. Le and N. V. Hieu, "Enhancement Of Gas-Sensing Characteristics Of Hydrothermally Synthesized WO_3 Nanorods By Surface Decoration With Pd Nanoparticles", *Sensors and Actuators B*, vol. 223, pp.453–460, 2016.

[10] J. Zhang, X. Liu, M. Xu, X. Guo, S. Wu, S. Zhang and S. Wang, "Pt Clusters Supported On WO_3 For Ethanol Detection", *Sensors and Actuators B*, vol. 147, pp. 185–190, 2010.

[11] Y. Wang, B. Liu, S. Xiao, H.L., L. Wang, D. Cai, D. Wang, Y. Liu, Q. Li and T.Wang, "High Performance And Negative Temperature Coefficient Of Low Temperature Hydrogen Gas Sensors Using Palladium Decorated Tungsten Oxide", *J. Mater. Chem. A*, vol. 3, pp.1317- 1324, 2015.

[12] S.B. Upadhyay, R.K. Mishra and P.P. Sahay, "Enhanced Acetone Response In Co-Precipitated WO_3 Nanostructures Upon Indium Doping", *Sensors and Actuators B*, vol. 209, pp. 368–376, 2015.

[13] P. Mohanapriya, R. Pradeepkumar, N. V. Jaya and T. S. Natarajan, "Magnetic And Optical Properties Of Electrospun Hollow Nanofibers Of SnO_2 Doped With Ce-Ion", *Applied Physics Letters*, vol. 105, pp. 22406-22410, 2014.

[14] H.P. Klug, L.E. Alexander, *X-Ray Diffraction Procedures For Polycrystalline And Amorphous Materials*, Wiley, New York, 1974.

[15] K. Anand, J. Kaur, R.C. Singh and R. Thangaraj, "Structural, Optical And Gas Sensing Properties Of Pure And Mn-Doped In_2O_3 Nanoparticles", Ceramics International, vol. 42, pp. 10957–10966, 2016.

[16] F. Mehmood, J. Iqbal, T. Jan, W.Ahmed, W. Ahmed, A. Arshad, Q. Mansoor, S. Z. Ilyas, M. Ismail and I. Ahmad, "Effect Of Sn Doping On The Structural, Optical, Electrical And Anticancer Properties Of WO_3 Nanoplates"*Ceramics International*, vol. 42, pp. 14334–14341, 2016.